Reprinted from ENVIRONMENTAL SCIENCE & TECHNOLOGY, Vol. 29, 1995

Coupled Iron Corrosion and Chromate Reduction: Mechanisms for Subsurface Remediation

ROBERT M. POWELL,*,† ROBERT W. PULS,‡ SHARON K. HIGHTOWER,† AND DAVID A. SABATINI§

ManTech Environmental Research Services Corporation, P.O. Box 1198, Robert S. Kerr Environmental Research Laboratory, 919 Kerr Research Drive, Ada, Oklahoma 74821-1198, U.S. Environmental Protection Agency, Robert S. Kerr Environmental Research Laboratory, 919 Kerr Research Drive, Ada, Oklahoma 74821-1198, and Department of Civil Engineering and Environmental Science, University of Oklahoma, 202 West Boyd, Norman, Oklahoma 73019

The reduction of chromium from the Cr(VI) to the Cr(III) state by the presence of elemental, or zero-oxidation-state, iron metal was studied to evaluate the feasibility of such a process for subsurface chromate remediation. Reactions were studied in systems of natural aquifer materials with varying geochemistry. Different forms of iron metal had significantly different abilities to reduce chromate, ranging from extremely rapid to essentially no effect. Impure, partially oxidized iron was most effective, with iron quantity being the most important rate factor, followed by aquifer material type and solid:solution ratio. Evidence for chromium–iron hydroxide solid solution $(Cr_X,Fe_{1-X})(OH)_3(ss)$ formation was obtained by electron probe microanalysis. A cyclic, multiple reaction electrochemical corrosion mechanism, enhanced by the development of an electrical double-layer analogue, is proposed to explain the differing iron reactivities and aquifer material effects.

Introduction

Chromium is a commonly identified groundwater contaminant, particularly in industrialized areas (*1*, *2*). Remediating chromate *in situ* by reduction and immobilization is desirable due to pump-and-treat limitations (*3*) and the expense of discarding surface treatment wastes. One proposed technique involves fabricating permeable and reactive subsurface barriers to prevent contaminant migration by sorption, precipitation, or biotransformation as it passes through the barrier and is exposed to altered pH, redox, sorptive substrates, or biotic activity (*4*–*7*). Elemental or zero-oxidation-state metals have been proposed for use in such barriers to reductively dehalogenate organic compounds such as trichloroethene (TCE) and tetrachloroethene (PCE) (*8*, *9*).

In aqueous systems, the distribution of chromium forms is strongly dependent on pH and E_h (*10*). It occurs in two stable oxidation states in the subsurface environment, Cr(VI) and Cr(III) (*11*, *12*). Under oxic conditions Cr can exist as Cr(VI) oxyanions, $HCrO_4^-$ (bichromate ion) at pH ≤ 6 and CrO_4^{2-} (chromate ion) at pH > 6 (*13*). These oxyanions are readily reduced to trivalent forms by electron donors such as organic matter or reduced inorganic species. The reduction rate increases with decreasing pH (*14*). Cr(III) species are dominated by $CrOH^{2+}$ in the pH range 4–6.5, with $Cr(OH)_3^0$ forming in the pH range 6.5–10.5 (*15*). The Cr(III) forms are very stable with respect to E_h, except in the presence of oxidized Mn (*16*–*18*), and are not oxidized by atmospheric O_2 until pH > 9 (*19*). The chromate forms are of greatest environmental concern due to their toxic and carcinogenic properties (*13*) and their greatly increased subsurface mobility compared to the relatively immobile and nontoxic Cr(III) and its species (*20*).

When reduced, Cr is removed from solution as $Cr(OH)_3^0$, a precipitated phase, or when dissolved iron is present, potentially as a chromium–iron hydroxide solid solution $(Cr_X,Fe_{1-X})(OH)_3(ss)$ (*15*). The formation of this solid solution is desirable for remediation. When the components of a solid solution are homogeneously mixed and fit readily into the crystalline structure, without tending to be expelled, they will have lower equilibrium solution activities than pure solid phases. This is because component activities at the surface of such a solid solution are less than unity (*21*–*23*). Cr^{3+} and Fe^{3+} meet the crystalline structure criteria, having the same charge and nearly the same ionic radii, 0.63 and 0.64 Å, respectively (*24*). Therefore, precipitated Cr is more insoluble in this form.

Research investigating CrO_4^{2-} reduction by iron has focused on ferrous ions in solution (*25*) and the presence of ferrous iron-bearing minerals (*26*, *27*). In such systems, a redox couple forms where Fe^{2+} is oxidized to Fe^{3+} and Cr^{6+} is reduced to Cr^{3+}. Zero-valence-state metals can also serve as electron donors for the reduction of oxidized species under certain conditions. The thermodynamic instability (*28*–*30*) of the metal can drive oxidation–reduction reactions without external energy input, if suitable coupled reactions can occur to prevent accumulation of electric charge (*29*). CrO_4^{2-} can serve as the oxidant in such a system and become reduced. Blowes and Ptacek (*31*) have shown CrO_4^{2-} reduction in the presence of metallic iron filings and chips. A corrosion mechanism has been proposed to explain these systems (*32*–*34*). The primary requirement is the formation of an electrochemical corrosion cell (ECC) (*29*) and the onset of aqueous corrosion (*28*).

Objectives. This research had multiple objectives. These were to determine the following: (a) whether ECC formation was responsible for the removal of solution CrO_4^{2-} by elemental iron reported by Blowes and Ptacek (*31*); (b) if removal would occur in systems incorporating aquifer materials; (c) the rates and mechanisms of the CrO_4^{2-} removal; (d) the form and location of the removed chromium; (e) how iron type and geochemical differences

† ManTech Environmental Research Services Corporation.
‡ U.S. Environmental Protection Agency.
§ University of Oklahoma.

0013-936X/95/0929-1913$09.00/0

affect these reactions; (f) whether this remediation approach is suitable for a CrO_4^{2-} plume at the U.S. Coast Guard Air Support Center, Elizabeth City, NC (*35*). Since this work draws heavily on the ECC concept, its basic features will be briefly described in the following section.

Electrochemical Corrosion Cell. Zero-oxidation-state refined metals tend to revert to a more thermodynamically stable form; for example, Fe oxidizes to Fe_2O_3 in the earth's oxygen-rich atmosphere (*30*). When the metal is immersed in an aqueous salt solution, an electrochemical corrosion mechanism can occur. Electrons (e^-) are released in one area (the anodic region), forming metal cations, and taken up by oxidized species at another part of the metal surface (the cathodic region). This avoids the accumulation of electric charge. Such a cell can form (a) when dissimilar metals are connected (by contact, for example); one becomes the anode, the other the cathode; [Their position in the galvanic series determines the direction of e^- flow.] (b) when anodic and cathodic regions develop on the same metal surface. This can result from compositional variations within the metal, surface defects, grain structure orientation, stress differences, and chemical variations in the surrounding electrolyte solution (*28–30, 36*).

These are the external circuits of the cell. An internal circuit is also necessary, and this requirement is fulfilled by the electrolyte. The external circuit transfers e^- from the anode to the cathode where they can react with H^+ to form hydrogen gas, with O_2 and H^+ to form water and OH^-, or with other oxidized species, such as Cr^{6+}, to form Cr^{3+}. For example, when iron is the anode:

$$Fe^0 \rightleftharpoons Fe^{2+} + 2e^- \quad \text{anode} \quad (1)$$

$$2H^+ + 2e^- \rightleftharpoons H_2(g) \quad \text{cathode} \quad (2)$$

$$Fe^0 + 2H^+ \rightleftharpoons Fe^{2+} + H_2(g) \quad \text{net reaction} \quad (3)$$

and when oxygen is present:

$$Fe^0 \rightleftharpoons Fe^{3+} + 3e^- \quad \text{anode} \quad (4)$$

$$6H^+ + 1.5O_2 + 3e^- \rightleftharpoons 3OH^- + 1.5H_2 \quad \text{cathode} \quad (5)$$

$$Fe^0 + 1.5O_2 + 6H^+ \rightleftharpoons Fe(OH)_3 + 1.5H_2 \quad \text{net reaction} \quad (6)$$

or should CrO_4^{2-} be available:

$$Fe^0 \rightleftharpoons Fe^{3+} + 3e^- \quad \text{anode} \quad (7)$$

$$CrO_4^{2-} + 4H_2O + 3e^- \rightleftharpoons Cr(OH)_3 + 5OH^- \quad \text{cathode} \quad (8)$$

$$Fe^0 + CrO_4^{2-} + 4H_2O \rightleftharpoons Fe(OH)_3 + Cr(OH)_3 + 2OH^- \quad \text{net reaction} \quad (9)$$

The dominant reactions will depend on geochemical conditions. These reactions all increase the pH of the corrosion system. Equation 9 implies that $(Cr_X,Fe_{1-X})(OH)_3$(ss) solid solution (*15*) is a possible result when CrO_4^{2-} is present.

Experimental Section

Aquifer Core Materials. The aquifer material used for most experiments was from the U.S. Coast Guard Air Support Center, Elizabeth City, NC. The site geology is Atlantic coastal plain sediment consisting of surficial sand, silt, and clay. An uncontaminated core was acquired near a chrome plating shop that had released acidic wastes into the subsurface via an eroded opening in the concrete floor (*35, 37*). The Elizabeth City (EC) material had a moisture content of 23 wt % with a mean particle size, $d_{50} \approx 0.17$ mm, and coefficient of uniformity, $d_{60}/d_{10} \approx 0.15/0.39 = 0.38$. Core material from Otis Air Force Base, Cape Cod, MA, was used to compare two distinct depositional environments. The Cape Cod (CC) sediment is composed of Pleistocene glacial deposits of sand and gravel with trace quantities of silt and clay sized particles (*38*). It was 0.62 wt % moisture with $d_{50} \approx 0.52$ mm and $d_{60}/d_{10} \approx 0.43/1.35 = 0.32$. Analyses for Al, Ca, Mg, Fe, and K indicated the presence of aluminosilicate clays in the EC, with far lower concentrations in the CC. A tested silica sand (CSSI) was a 10–20 mesh fraction and was not further characterized.

Iron Metals. Scrap iron filings from Ada Iron and Metal (AI&M), Ada OK, were the most comprehensively studied of the Fe^0-bearing metals and by far the most reactive. This Fe was not pure and was visually observed to be partially oxidized. Cast iron metal chips were obtained from Master Builder's Supply (MBS), Streetsboro, OH. The metals were repeatedly washed with 7 mM NaCl in deionized water and freeze-dried. Chemical analysis showed that both could be classified as low-grade steels. BET surface areas were 8.26 m^2/g for the AI&M and 1.10 m^2/g for the MBS.

Stirred Batch Reactors. Stirred batch reactor (SBR) experiments were performed in 500-mL Fleakers (*32–34*). In general, these contained simulated aquifer water (SAW) and AI&M Fe^0 in the presence or absence of aquifer material. A solid:solution ratio of 150 g of aquifer material:350 g of SAW was used when aquifer material was present. Both EC and CC were used in their cored and naturally wet states. The SAW simulated the average major ionic composition of the Elizabeth City site ($CaSO_4$ = 1 mM, NaCl = 7 mM, pH = 6.5) or the Cape Cod site ($CaSO_4$ = 0.14 mM, NaCl = 0.49 mM, pH = 5.9). The Elizabeth City SAW was used with the CSSI silica sand for comparison purposes. A humidified N_2 blanket was maintained above the SBRs to mimic the oxygen depletion that might occur within a subsurface reactive barrier (eqs 5 and 6). Reaction temperatures were 25 ± 2 °C.

E_h, pH, and system temperature were continuously acquired by Orion 290A pH/ion selective electrode meters and recorded by computers. The redox electrode was a Corning combination with an Ag|AgCl reference and a Pt disk. The pH electrode was an Orion Triode, with built-in temperature probe. The electrodes, N_2 outlet, and stirring paddle were rigidly suspended through the Fleaker opening. The stirring rate kept all solid phase materials suspended. Reactors were wrapped with foil to prevent light-induced reactions (*39*) and more closely simulate the subsurface.

Initially, the SBRs contained only SAW or SAW plus aquifer material. After 48 h to let the SBRs approach pseudo-equilibrium with respect to pH and E_h, 8 g of washed and freeze-dried N_2 purged AI&M Fe filings were added. At about 60 h, stock K_2CrO_4 solution was added to give initial aqueous CrO_4^{2-} concentrations of 136–156 mg Cr/L. For one type of experiment, CrO_4^{2-} was added rather than Fe at $t \approx 48$ h and, after 115 h, 8 g of N_2-purged AI&M Fe was added.

E_h and pH were monitored at 10–15-s intervals following the Fe and CrO_4^{2-} additions. Samples were withdrawn both before and after the additions and were immediately filtered through preweighed 0.2 μm pore diameter Gelman Nylaflo

membrane filters under vacuum. An aliquot of the filtrate was removed for SO_4^{2-} and Cl^- analysis by capillary electrophoresis (CE). The remaining filtrate was acidified to pH < 2.0 with HNO_3 and analyzed by inductively-coupled plasma emission spectroscopy (ICP). Solids and filters were dried at 70 °C, digested, and analyzed by ICP. Polished epoxy briquettes of solid phase materials from the SBRs were prepared for electron probe microscopy (EPM) (*40*). Color-enhanced element maps were generated to compare spatial codistributions of elements and deduce primary solid compound stoichiometries.

Shaken Batch Bottles. To evaluate effects of the variables aquifer material, solid:solution ratio, iron, and $[SO_4^{2-}]$, shaken batch bottle experiments (SBBs) were used. A pseudofactorial design was employed to reduce the number of replicates and repeated variables. These experiments were done in shaken Oak Ridge polyallomer centrifuge tubes in a N_2-filled glovebox. They were set up with five concentrations or masses of each variable, in duplicate.

Tubes of SAW and aquifer material were secured horizontally on a Thermolyne Maxi-Mix III rotating shaker at 300 rpm and equilibrated for 24 h. E_h and pH were then measured in the glovebox, Fe metal was added, and the samples were returned to the shaker. After 48 h, E_h and pH were again measured, and CrO_4^{2-} was added ($t_0 = 0$) to give a concentration of 126 mg of Cr/L. The tubes were sampled in the glovebox at t = 20 min, 2, 7, 24, 48, and 96 h. Samples were immediately filtered and analyzed as given previously for the SBRs.

Chromate Adsorption/Desorption Experiments. Chromate adsorption isotherms were performed on both the naturally wet and dried forms of the EC material (*34, 36, 41, 42*). The isotherms were generated by batch experiments with constant EC masses and solution volumes (7mM NaCl) with five levels of CrO_4^{2-} concentration at pH = 6.5. Batches were shaken for 24 h and then centrifuged at 1500 rpm for 30 min. Centrates were acidified with HNO_3 for analysis by ICP. Chromate desorption, using high phosphate concentrations to compete for adsorption sites (*34, 35, 43–45*), was used to assure that CrO_4^{2-} was reduced in these systems rather than merely adsorbed to the iron oxyhydroxide rusts that are formed.

Results and Discussion

Chromate Adsorption/Desorption. Adsorption data (*34*) were modeled using the Freundlich equation. The dried EC exhibited greater Cr adsorption than the naturally wet material with less surface saturation at the concentrations used. This was possibly due to adsorption by Fe forms that were oxidized during the drying process. The Freundlich K_{fr} for the chromate Cr adsorption was 3.4 mL/g for the dry composite (n = 0.80) and 2.8 mL/g for the wet material (n = 0.91). Adsorption capacity (b) was estimated with the Langmuir equation (*46*). For the wet EC material b = 24.3 μg of chromate Cr/g with K_L = 0.147. For the dry EC, b = 34.5 μg of chromate Cr/g with K_L = 0.112.

The competitive desorption of CrO_42- from surface adsorption sites by excess PO_4^{3-} resulted in nearly full recovery of initial Cr concentrations in all experiments without Fe^0 (*34*). However, samples containing Fe^0 were reduced from 109 mg of Cr/L to below 0.3 mg/L with no CrO_4^{2-} recovery by PO_4^{3-} desorption. This confirmed that reduction was occurring and not adsorption by oxyhydroxides.

Stirred Batch Reactors. If corrosion occurs, the E_h at the surface of the corroding anode should approach that of the oxidation–reduction half-reaction responsible for the dissolution of the metal surface (eqs 1, 4, and 7). Effects on pH should also indicate the system's behavior. In a suspension, bulk E_h and pH should approach those near the reactive surface. This is the entire reactive surface, however, including both cathodic and anodic regions. Therefore the half-reactions of the electron acceptors (e.g., eqs 2, 5, and 8) will also influence the measured E_h and pH as will any other active redox couples. This is called a mixed potential.

Figures 1 and 2 compare the E_h and pH results of type 1 and type 2 SBR experiments using 8 g of AI&M Fe^0 without and with EC aquifer material, respectively. When Fe^0 is added, the E_h rapidly drops to negative values in both systems, indicating greatly increased e^- activity, while pH rises. This is indicative of corrosion reactions (eqs 1–9). When CrO_4^{2-} is added, pH again rises and E_h reverses to become more positive, but not as positive as before the Fe^0 addition. The pH increase is predicted by eq 9, and the intermediate E_h illustrates a mixed potential. The plots as well as visual observation of oxyhydroxide rust formation indicate that corrosion reactions are occurring, since the E_h values following the addition of Fe^0 were driven to values approaching the half-reaction potential

$$Fe^{2+} + 2e^- \leftrightarrow Fe(s) \qquad E^\circ = -447 \text{ mV (ref 24)} \qquad (10)$$

and the CrO_4^{2-} addition moved the mixed potential in the direction

$$CrO_4^{2-} + 4H_2O + 3e^- \leftrightarrow Cr(OH)_3(s) + 5OH^-$$
$$E^\circ = 400 \text{ mV (pH = 9) to } E^\circ = 560 \text{ mV (pH = 7)} \quad \text{(ref 13)} \quad (11)$$

The initial E_h changes upon Fe^0 addition provide additional evidence for corrosion; these were best fit by zero-order reactions (*34*). Zero-order kinetics imply that the rates of E_h change were not significantly impacted by the reactant concentrations generating the initial e^- activity. This is probably because the 8 g of Fe^0 filings approximated an infinite reactive surface area with respect to the corrosion coupling, solubilization, and instantaneous redox capacities of the SAW solution. This partially oxidized and impure Fe material may have carried, on its surface and in its composition, all the redox couples needed to initiate the corrosion process, lacking only the internal circuit (i.e., the solution) to complete the electrochemical cell.

The total E_h and pH changes in the type 2 experiment (Figure 2) were not as extreme as those of the type 1 (Figure 1). In addition, the rates of E_h change were reduced by nearly an order of magnitude with EC material present (type $1_{av} \approx 3900$ mV min^{-1}, type $2_{av} \approx 500$ mV min^{-1}). These results indicate that EC has buffering capacity for both parameters. This is significant for CrO_4^{2-} reduction, since the reaction rate increases with lower pH but decreases with increasingly positive E_h.

Figure 2 (EC material present) shows a stable post-CrO_4^{2-} addition pH = 7.5. Solution CrO_4^{2-} was reduced below detection limits (0.0024 mg of Cr/L) within 60 h. Its disappearance corresponded to the E_h drop that occurred at that point, i.e., the diminishment of this particular mixed

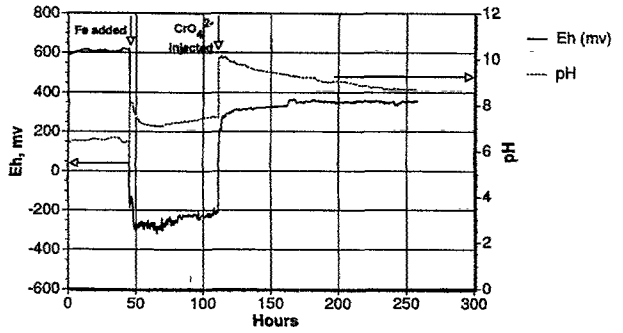

FIGURE 1. Type 1 stirred batch reactor E_h and pH results, using AI&M Fe, no aquifer material.

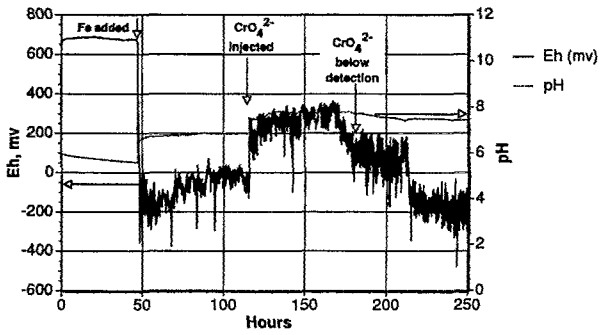

FIGURE 2. Type 2 stirred batch reactor E_h and pH results, using AI&M Fe, Elizabeth City aquifer material.

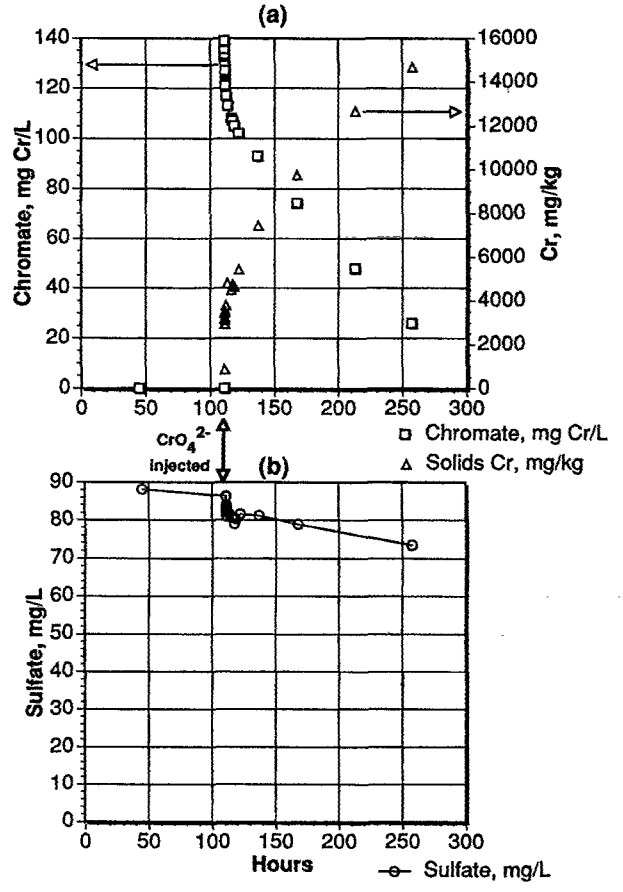

FIGURE 3. Chromate (a) and sulfate (b) behavior in the type 1 stirred batch reactor with no aquifer material.

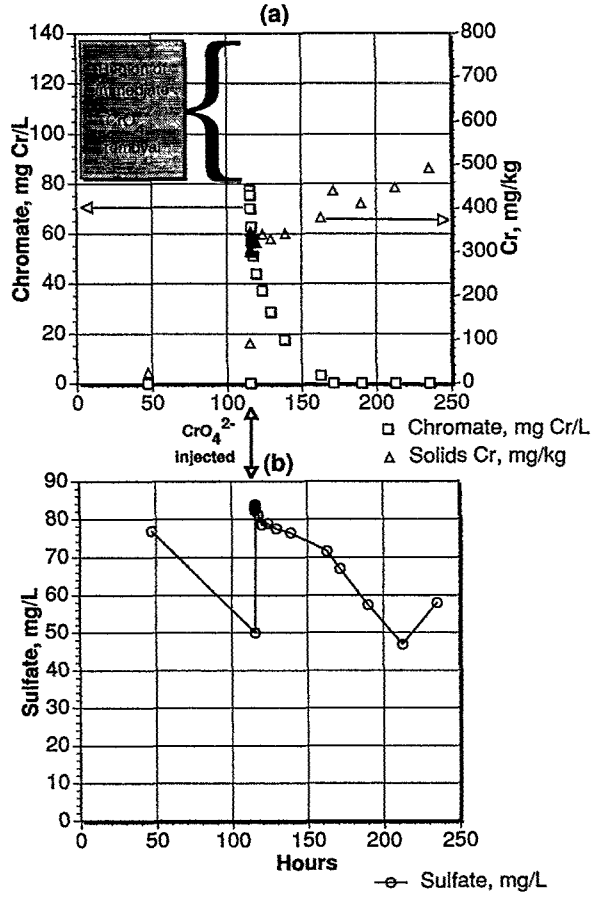

FIGURE 4. Chromate (a) and sulfate (b) behavior in the type 2 stirred batch reactor with Elizabeth City aquifer material.

potential. This drop indicated continuing corrosion and Fe dissolution, even in the absence of CrO_4^{2-} as an electron acceptor.

In Figure 1 (EC material absent), the pH never fell below 8.7 after CrO_4^{2-} addition. CrO_4^{2-} was not completely reduced during the 146 h following its addition, and the E_h drop did not occur.

Data from an EC-containing SBR where Fe^0 was added after the CrO_4^{2-} rather than before supported the idea that electron acceptors are available from the EC material. Chromate disappeared rapidly upon Fe^0 addition while E_h declined and remained low, due to continuing reactions at lower E° than eq 11 (e.g., $2H^+ + 2e^- \leftrightarrow H_2$ at $E^0 = 0.00$ V). Sieve analyses (*34*) indicated significantly more fines in the EC than in either the CC or 10–20 mesh CSSI materials. It is likely that these fines were contributing electron acceptors to couple with the corrosion reactions, possibly via hydrolysis and secondary proton-generating reactions.

Figure 3a (type 1, EC absent) shows significant but incomplete solution CrO_4^{2-} removal, from 140 initially to 26 mg Cr/L by experiment's end, along with Cr appearance in the solid phase. When EC material was present (Figure 4a) CrO_4^{2-} was removed within 1 min to ≈80 mg Cr/L and completely eliminated within 50 h. Using the Langmuir capacity term b, it was estimated that only 6.7% of the added Cr could be removed by adsorption to EC material at pH = 6.5 (natural aquifer pH). At a reactor pH of 7.5 the EC solids would have even greater net negative charge, decreasing adsorption of negatively charged CrO_4^{2-} below the Langmuir estimates. Thus, the instantaneous loss was not due solely to adsorption onto the aquifer material.

TABLE 1

Shaken Batch Bottles Using Elizabeth City Aquifer Material[a]

	Fe type	Fe (g)	aq mat (g)	sulfate (mM)	solid:solution	final Cr (mg/L)	K (h^{-1})	$t_{1/2}$, (h)
EC1A	AI&M	*0*	9	0.86	0.35	104	-6.20×10^{-4}	1118
EC1B	AI&M	*0.01*	9	0.86	0.35	85	-2.16×10^{-3}	320
EC1C	AI&M	*0.05*	9	0.86	0.35	79	-2.40×10^{-3}	289
EC1D	AI&M	*0.1*	9	0.86	0.35	52	-5.86×10^{-3}	118
EC1E	AI&M	*0.25*	9	0.86	0.35	<0.020	-5.66×10^{-2}	12
EC2A	AI&M	0.48	*0*	0.86	0	<0.020	-1.75×10^{-1}	3.9
EC2B	AI&M	0.48	*0.05*	0.86	0.002	<0.020	-8.28×10^{-2}	8.4
EC2C	AI&M	0.48	*0.5*	0.86	0.02	<0.020	-1.57×10^{-1}	4.4
EC2D	AI&M	0.48	*5*	0.86	0.2	<0.020	-1.26×10^{0}	0.6
EC2E	AI&M	0.48	*20*	0.86	0.77	<0.020	-1.54×10^{0}	0.4
EC3A	AI&M	0.48	9	*0.1*	0.35	<0.020	-2.79×10^{-1}	2.5
EC3B	AI&M	0.48	9	*1.1*	0.35	<0.020	-3.06×10^{-1}	2.3
EC3C	AI&M	0.48	9	*2.1*	0.35	<0.020	-3.05×10^{-1}	2.3
EC3D	AI&M	0.48	9	*3.1*	0.35	<0.020	-3.02×10^{-1}	2.3
EC3E	AI&M	0.48	9	*4.1*	0.35	<0.020	-3.00×10^{-1}	2.3
EC4A	MBS	*0*	9	5.9	0.35	110	-5.23×10^{-4}	1325
EC4B	MBS	*0.01*	9	5.9	0.35	109	-9.71×10^{-4}	714
EC4C	MBS	*0.05*	9	5.9	0.35	105	-1.02×10^{-3}	679
EC4D	MBS	*0.1*	9	5.9	0.35	99	-1.40×10^{-3}	493
EC4E	MBS	*0.25*	9	5.9	0.35	102	-1.36×10^{-3}	508
EC5A	MBS	0.48	*0*	5.9	0	98	-4.01×10^{-3}	173
EC5B	MBS	0.48	*0.05*	5.9	0.002	94	-3.72×10^{-3}	186
EC5C	MBS	0.48	*0.5*	5.9	0.02	92	-3.32×10^{-3}	209
EC5D	MBS	0.48	*5*	5.9	0.2	82	-4.05×10^{-3}	171
EC5E	MBS	0.48	*20*	5.9	0.77	64	-6.31×10^{-3}	110

[a] Negative K values indicate loss of chromate from solution. [b] Variables in italics.

However, due to corrosion, the type 2 reactor had generated a large quantity of iron oxyhydroxides, greatly increasing the potential adsorption capacity of the system (*43*, *47*). The type 1 experiment had the same initial mass of Fe^0 and contained oxyhydroxides, but no instantaneous CrO_4^{2-} loss was observed. This difference can be explained by system pH. The iron solid phase most likely to form initially is amorphous $Fe(OH)_3$, with a $pH_{zpc} \approx 8.5$. Therefore, at pH = 7.5 in the type 2 experiment, a large surface area of $Fe(OH)_3$ with a net positive charge was present, allowing significant CrO_4^{2-} adsorption. In the type 1 experiment, the pH had risen to 10.3 and never fell below 8.7, significantly higher than the pH_{zpc} of $Fe(OH)_3$. This greatly reduced the number of positively charged surface sites and instantaneous CrO_4^{2-} adsorption was not observed. These observations are supported by SO_4^{2-} behavior. In Figure 3b, a small amount of SO_4^{2-} adsorption occurred following Fe^0 addition. Figure 4b, however, shows significant SO_4^{2-} adsorption following Fe^0 addition, with its immediate desorption upon competition by the approximately equimolar CrO_4^{2-}. This was followed by gradual SO_4^{2-} readsorption as the CrO_4^{2-} was reduced. It is not known whether reduction of adsorbed CrO_4^{2-} made existing adsorption sites available for SO_4^{2-} readsorption or if this was due to the production of new adsorption sites as fresh iron oxyhydroxide rust was formed by corrosion.

An SBR using CSSI silica sand also completely reduced CrO_4^{2-} but did not show instantaneous CrO_4^{2-} adsorption (pH > 8.5) or the extent of SO_4^{2-} adsorption and desorption seen in the EC type 2 study. The E_h drop following CrO_4^{2-} reduction was also not as significant. This signaled the absence of electron acceptors and the decline of the corrosion reactions that had provided reduced species to the solution.

Reduction rates in all SBRs were adequately described by pseudo-first-order reactions with respect to Cr, indicating a concentration dependence on CrO_4^{2-} or the reduction mechanism(s). Reduction occurred more rapidly when EC aquifer material was present ($t_{1/2}$ = 10.8 h) than when either CC ($t_{1/2}$ = 15.8 h) or CSSI ($t_{1/2}$ = 14.6 h) materials were used. With no aquifer material (type 1 SBR), the rate was much slower ($t_{1/2}$ = 67.9 h).

Shaken Batch Bottles (SBB). Table 1 presents the setup, final Cr concentrations, and first-order $t_{1/2}$ results for five types of batch experiments with EC material. Sample codes 1, 2, 3, 4, or 5 followed by A through E indicate the batch type (i.e., the variable parameter) and the level of the variable, respectively. Variable parameter values are in italics. Experiments were also conducted with CC and CSSI materials; these results are presented elsewhere (*34*).

Effect of Iron. Increased Fe^0 mass decreased $t_{1/2}$ values. This effect was greatest for the AI&M Fe^0 and most pronounced in the presence of EC materials (Figure 5a; Table 1, EC1). The MBS Fe^0 had much lower reactivity (Figure 5b; EC4). This could be partially due to its lower surface area relative to the AI&M, but this factor of 8 could not account for the differences. In addition, extremely slow CrO_4^{2-} reduction by pure Fe^0 has been shown (*34*). Although some Fe^{2+} dissolution may have gradually occurred and reduced small amounts of CrO_4^{2-}, a new or enhanced mechanism occurred when EC material was added, even in small quantities. This supports the hypothesis that the AI&M Fe^0 carried all redox couples needed to initiate the corrosion process. The pure Fe^0 did not and very little happened when EC material was absent.

Effect of Aquifer Material Type. The EC material caused some loss of solution CrO_4^{2-} due to adsorption and some natural reductive capacity, even with no Fe^0 present (Table 1, EC1A, EC4A; Figure 5a,b). A loss from 126 to 114 mg of Cr/L can be predicted from the Langmuir capacity term, which would include both effects. Figure 5 shows that all EC systems removed Cr from solution to at least 114 mg/L

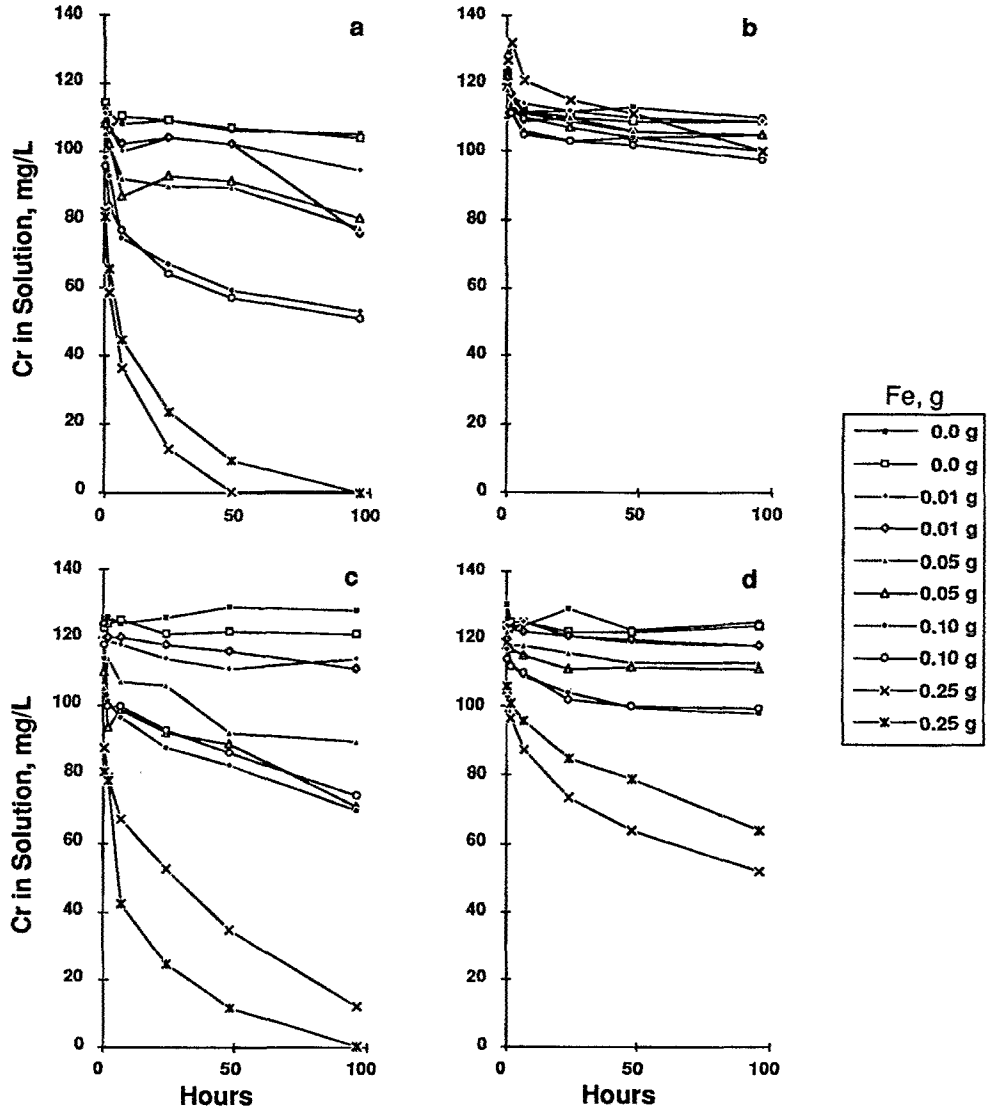

FIGURE 5. Cr in solution versus time for (a) SBB EC1: Elizabeth City aquifer material and AI&M Fe, (b) SBB EC4: Elizabeth City aquifer material and MBS Fe, (c) SBB CC1: Cape Cod aquifer material and AI&M Fe, and (d) SBB SS1: commercial silica sand and AI&M Fe.

by the first sampling at $t = 20$ min (0.33 h). Both EC and CC systems completely reduced CrO_4^{2-} when sufficient AI&M Fe^0 was present, but when less Fe^0 was available, the EC material was more effective. CSSI sand (Figure 5d) compared poorly to either EC1 or CC1.

The EC material buffered pH to lower values. As was shown, a stable SBR reaction pH = 7.5 was attained using EC material, while CC and CSSI yielded pH ≈ 8.7. Pourbaix (*48*) has noted that iron corrosion progressively increases in intensity at pH < 9.5 or pH > 12.5, with the region between these values near the boundary of a domain of immunity. Therefore, corrosion "intensity" and, consequently, CrO_4^{2-} reduction should be enhanced by the lower pH of the EC systems. Figure 6 shows that the pH trends observed in the SBRs were also seen in the SBBs. These data were acquired just before the CrO_4^{2-} addition. Increasing AI&M Fe^0 mass from 0 to 0.25 g, at a constant 9 g of EC, increased pH about 1 unit (Figure 6a, left). Using CC material, pH increased approximately 1.7 pH units (Figure 6b, left). With constant Fe^0 = 0.48 g and aquifer material mass increased from 0 to 20 g, pH decreased only to pH ≈ 8.1 with CC (Figure 6b, right) but decreased to pH ≈ 7.2 with EC (Figure 6a, right). These data confirm that the EC had significantly more capacity to lower pH.

One explanation for the pH reduction is the larger quantity of aluminosilicate clay-sized particles in the EC materials. Aluminum and silica released by dissolution could be important in maintaining the corrosion reactions. Feldspar dissolution in systems far from equilibrium has been measured (*49*, *50*), and significant montmorillonite dissolution has been demonstrated at pH values bracketing those found in this study (*51*). Kaolinite dissolution under similar conditions can result in theformation of silicic acid and gibbsite (*21*). The gibbsite can then solubilize since $Al(OH)_4^-$ is the dominant solution Al species at pH > 7.

$$\underset{\text{kaolinite}}{Al_2Si_2O_5(OH)_4} + 7H_2O \rightarrow 2Al(OH)_4^- + 2H_4SiO_4 + 2H^+ \quad (12)$$

This yields silicic acid and protons. Below pH ≈ 9, dissolved silica exists primarily as H_4SiO_4. Silicic acid reactions with mineral surfaces such as goethite (α-FeOOH) release protons under alkaline conditions. This causes a shift in

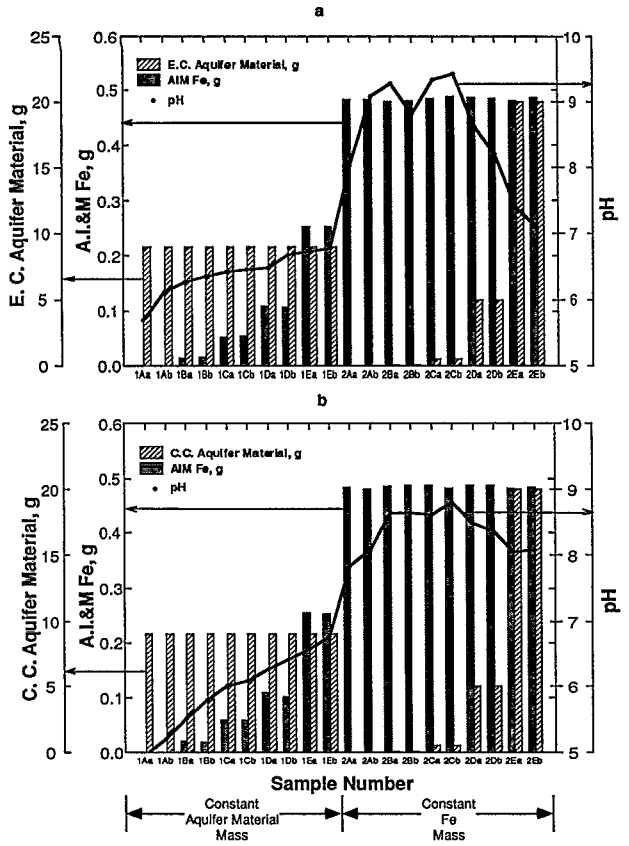

FIGURE 6. pH trends in the SBB experiments with (a) Elizabeth City and (b) Cape Cod aquifer materials.

the titration curve (*21*) that can be explained by reactions such as

$$\equiv FeOH + H_4SiO_4 \leftrightarrow \equiv FeOSi(OH)_3 + H_2O \quad (13)$$

$$\equiv FeOSi(OH)_3 \leftrightarrow \equiv FeOSiO(OH)_2^- + H^+ \quad (14)$$

The protons from eqs 12 and 14 can then become the needed electron acceptors for the corrosion processes to proceed.

Equations 13 and 14 are significant since corrosion reactions generate substantial iron oxyhydroxides. Coordination of silicic acid with these surfaces would reduce the solution H_4SiO_4 concentration, promoting additional aluminosilicate dissolution through disequilibrium. This dissolution would result in new protons, continued corrosion, and the formation of additional oxyhydroxides. Therefore, the EC aluminosilicates may yield protons via multiple and cyclic mechanisms, lowering pH and promoting CrO_4^{2-} reduction by proton coupling to corrosion reactions at the cathode (eq 2).

Effect of Solid:Solution Ratio. Increasing the EC solid:solution ratio generally enhanced CrO_4^{2-} reduction rates (Table 1, EC2, EC5). Calculations show this was not due simply to raising the total natural EC adsorption/reduction capacity in AI&M Fe^0-containing systems. However, when MBS Fe^0 was used (EC5), the difference between final CrO_4^{2-} concentrations for 5 (EC5D) and 20 g (EC5E) of EC material could be attributed to removal by the larger EC mass with little, if any, reduction by the iron. Reaction kinetics for all MBS samples (EC4, EC5) were nonlinear and seemed to consist of two or more limited-capacity mechanisms. These could be rapid adsorption onto the EC material followed

Multiple Regression Model

Dependent variable is:Log t1/2
No Selector
R squared = 94.5% R squared (adjusted) = 93.5%
s = 0.2671 with 15 - 3 = 12 degrees of freedom

Source	Sum of Squares	df	Mean Square	F-ratio
Regression	14.6207	2	7.31036	102
Residual	0.856032	12	0.071336	

Variable	Coefficient	s.e. of Coeff	t-ratio	prob
Constant	3.14248	0.1965	16.0	≤ 0.0001
Fe (g)	-5.15020	0.3602	-14.3	≤ 0.0001
Solid:Solution	-1.28123	0.3795	-3.38	0.0055

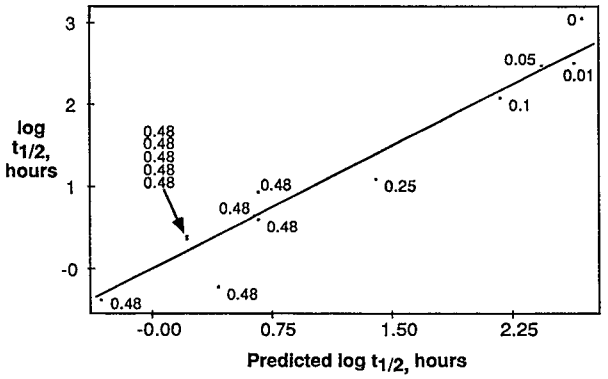

FIGURE 7. Whole model regression incorporating the effects of Fe in grams and solid:solution ratio. Plot illustrates the actual $t_{1/2}$ data versus the $t_{1/2}$ predicted by the model. Data point labels are iron mass in grams.

by its slightly slower natural CrO_4^{2-} reduction. The $t_{1/2}$ for the MBS Fe^0 samples are, therefore, biased to unrealistically short periods. Increases in the CC solid:solution ratio did not have a discernible effect on CrO_4^{2-} removal. This material also did not have any significant natural capacity to adsorb or reduce CrO_4^{2-}. This lack of capacity may be due to the absence of a significant clay-size fraction.

Sulfate Effects. Sulfate concentration had no apparent effect on CrO_4^{2-} reduction with EC material (Table 1, EC3). High concentrations enhanced CC systems, but the effect was minor, and these heterogeneous systems require caution when interpreting small data differences. Sulfate may form aqueous complexes of $FeSO_4$ with ferrous iron at low E_h, as predicted by Minteq A2 (*34*). Complexation could promote iron dissolution and stabilize reduced species to greater distances from the iron surfaces, enhancing CrO_4^{2-} reduction. None of the laboratory experiments achieved e^- activity sufficient to reduce SO_4^{2-}.

Analysis of the Elizabeth City SBB Half-Life Results. Exploratory data analysis was performed on the SBB experiments (*52*). The resultant multiple regression model and associated statistics are given with Figure 7, which shows predicted log $t_{1/2}$ versus the actual log $t_{1/2}$ values. Approximately 94% of the variation in the log $t_{1/2}$ is explained by AI&M Fe^0 mass and solid:solution. This model allows the time required for CrO_4^{2-} reduction by AI&M Fe^0 in combination with the EC aquifer material to be reasonably well predicted if the mass of iron, the solid:solution ratio, and the system volume are known. It should be noted, however, that the highest experimental solid:solution ratios are far lower than those of an aquifer. In addition, larger proportions of iron relative to fill materials would be incorporated into a permeable reactive barrier wall. Reduction rates in such a field scenario should be much faster.

Proposed Geochemical Mechanisms. Figure 8a,b shows the EPM elemental X-ray maps for Fe and Cr oxyhydroxides, respectively, on a reacted AI&M Fe^0 filing. Based on the apparent perfect correspondence between the Fe and Cr

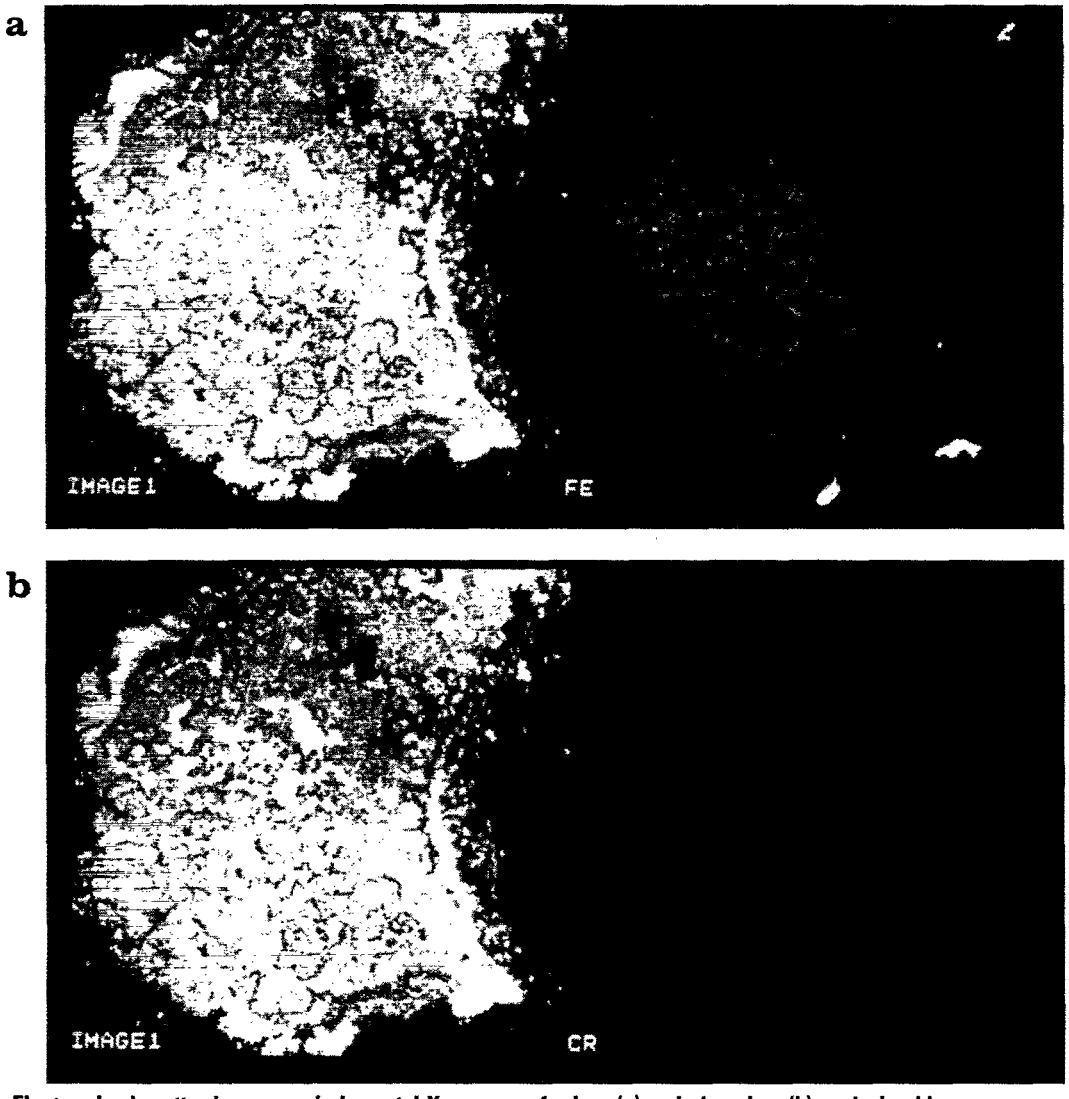

FIGURE 8. Electron backscatter images and elemental X-ray maps for iron (a) and chromium (b) oxyhydroxides.

phases, along with the literature, it seems certain that the Cr is being precipitated as $(Cr_X,Fe_{1-X})(OH)_3$ solid solution.

Figure 9 is a simplified representation of the near-Fe surface reactions that we propose are occurring in these nonequilibrium systems. It illustrates e^- movement in a corrosion cell domain on an iron filing. As represented, it appears to be a single, stable domain with clearly defined anodic and cathodic regions. This is possible; however, Scully (*28*) tells us that the metal surface often consists of continuously shifting anodic and cathodic sites. Oriented water molecules at the surface are not depicted because these are readily displaced by charged species since water molecules are polar but have no net charge (*29*).

Differences in the galvanic potentials of metals in the filing, other compositional variations, surface defects, grain structure orientation, stress differences, and/or chemical variations in the surrounding electrolyte result in e^- movement, forming anodic and cathodic regions within the corrosion cell domain. Electronically unstable zones bounding previously reacted/corroded surface areas will be susceptible to the formation of such domains. In these zones, dissolution is occurring and potentially unfilled orbitals exist alongside completely filled shells. The reactivity of these regions is derived from the concept of "active centers" on solid surfaces due to "unsaturated atoms" (*53*) and is implied by the quantum theory of solids (*54*). Reaction rates will be enhanced to a greater degree compared to pure, undeformed, atomically smooth surfaces. Due to e^- deficiency, the anodic region develops a net positive charge and surface Fe^{2+}. The Fe^{2+} is then free to enter the solution, its entry rate and solubility being dependent on solution chemistry.

We propose that in the vicinity of the positively charged anodic surface an analogue to the electrical double-layer model (*21*) will form. This would resemble a variable-charge mineral surface at a pH less than its pH_{zpc}. The surface/near-surface zone would resemble the Stern layer, with a swarm of anions (including CrO_4^{2-} and SO_4^{2-}) electrostatically drawn toward the surface and the released Fe^{2+}. This would promote formation of the $FeSO_4$ complex as well as redox coupling of CrO_4^{2-} to reduced Fe species, increasing the CrO_4^{2-} reduction rate. The simulated Gouy layer would be a diffuse zone dominated by cations as counterions to the Stern layer, gradating into the bulk solution.

The negatively charged cathodic region would resemble a variable-charge mineral at $pH > pH_{zpc}$. The Stern layer analogue would be dominated by cations, including protons (H^+) and other e^- acceptors as well as nonreducible ions

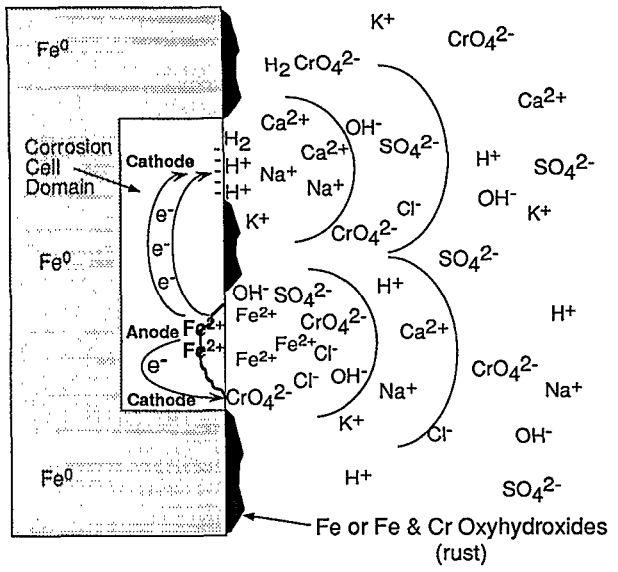

FIGURE 9. Graphical depiction of an iron or steel filing undergoing electrochemical corrosion; with electron transfer and the formation of anodic and cathodic regions within a corrosion cell domain, and the generation of electrical double-layer analogues at the surface and into the solution.

such as Na^+ and Ca^{2+}. The Gouy layer would be dominated by anions. At the cathodic surface, hydrogen ions are not strongly adsorbed, allowing some surface migration. As they approach one another they are reduced to diatomic molecules (H_2) and given off as a gas (*28*). These molecules can potentially couple with CrO_4^{2-} and cause its reduction, but H^+ is probably most important for maintaining the corrosion reaction by preventing charge accumulation and allowing iron dissolution. It might be considered unlikely that H^+ would be significant at neutral pH and above. Bulk pH and ionic concentrations cannot be considered fully representative of surface or corrosion pit conditions however (*28*). These experiments strongly suggest that protons have an important role in CrO_4^{2-} reduction by these reactions.

Another possible mechanism for CrO_4^{2-} reduction is direct e^- transfer at the iron surface. Although these experiments do not provide explicit evidence for this, the formation of positively charged surface regions along with the instantaneous but temporary adsorption of CrO_4^{2-} onto the freshly formed iron oxyhydroxides can keep CrO_4^{2-} near the surface. Shifting cathodic and anodic zones could allow a site with adsorbed CrO_4^{2-} to transfer e^- to the ion. Additional research is needed.

Summary and Conclusions

These data support the conclusion that CrO_4^{2-} in solution can be reduced to Cr(III) by corrosion mechanisms in the presence of elemental iron forms. These corrosion reactions can only proceed when suitable e^- acceptors are present to form an appropriate couple and prevent the accumulation of electric charge. Some types of iron are far more reactive than others for reducing CrO_4^{2-} while certain aquifer materials contribute more significantly to these reactions due to their mineralogy. Aluminosilicates appear able to provide e^- acceptors through dissolution, maintaining the corrosion process. A cycle can develop in which rust formation promotes additional dissolution. The Elizabeth City aquifer material had this capability; the Cape Cod and CSSI silica sand did not. Studies on the effects of clay type and concentration are continuing.

The CrO_4^{2-} plume at the Elizabeth City site should respond well to remediation by this method provided that native aquifer materials are mixed with the AI&M Fe^0 and backfilled to construct the reactive barrier(s). Commercial sands alone may not be sufficient for backfill without modification (such as the addition of clays) due to their inability to buffer pH and provide suitable chemical coupling.

Acknowledgments

Although the research described in this article was funded by the U.S. Environmental Protection Agency under Contract 68-C3-0322 to ManTech Environmental Research Services Corporation and under in-house research programs, it has not been subjected to Agency review and therefore does not necessarily reflect the views of the Agency, and no official endorsement should be inferred. The authors thank Lloyd Petrie, Dianne Marozas, Steve Paulson, and Mike Boucher of the U.S. Bureau of Mines, Twin Cities Research Center, Minneapolis, MN, for the excellent EPM analyses, report, and discussions. We also thank Don Clark and Guy Sewell (U.S. Environmental Protection Agency), Mark White, Priscilla Rhynes, and Lynda Pennington (ManTech Environmental Research Services Corp.), and Robert Knox (University of Oklahoma), all of whom made valuable contributions to this paper.

Literature Cited

(1) Robertson, F. N. *Ground Water* **1975**, *13*, 516–527.
(2) Sloof, R. F. M. J.; Cleven, J. A.; Van der Poel, J.; Van der Poel, P. *Integrated criteria document: Chromium*; RIVM-710401002; National Institute of Public Health and Environmental Protection: Bilthoven, The Netherlands, 1990.
(3) Keely, J. F. *Performance evaluations of pump-and-treat remediations*; EPA/540/4-89/005; U.S. Environmental Protection Agency, Robert S. Kerr Environmental Research Laboratory: Ada, OK, 1989.
(4) Spangler, R. R.; Morrison, S. J. *Environmental Restoration, ER-91*; U.S. Department of Energy: Pasco, WA, 1991.
(5) Morrison, S. J.; Spangler, R. R. *Environ. Sci. Technol.* **1992**, *26*, 1922–1931.
(6) Fruchter, J. S. *In Situ Redox Manipulation: Enhancement of Contaminant Destruction and Immobilization*; PNL-SA-21731; Pacific Northwest Laboratory: Richland, WA, 1993.
(7) Morrison, S. J.; Spangler, R. R. *Environ. Prog.* **1993**, *12*, 175–181.
(8) Gillham, R. W.; O'Hannesin, S. F. *IAH Conference on Modern Trends in Hydrogeology*; IAH: Hamilton, Ontario, Canada, 1992.
(9) O'Hannesin, S. F.; Gillham, R. W. *45th Canadian Geotechnical Society Conference*; Toronto, Ontario, Canada, 1992.
(10) Schmidt, R. L. *Thermodynamic Properties and Environmental Chemistry of Chromium*; PNL-4881; U.S. Department of Energy: Richland, WA, 1984.
(11) Calder, L. M. In *Chromium in the Natural and Human Environments*; Nriagu, J. O., Nieboer, E., Eds.; John Wiley & Sons: New York, 1988; Vol. 20, pp 215–229.
(12) McLean, J. E.; Bledsoe, B. E. *Behavior of Metals in Soils*; EPA/540/S-92/018; U.S. Environmental Protection Agency, Robert S. Kerr Environmental Research Laboratory: Ada, OK, 1992.
(13) Nieboer, E.; Jusys, A. A. In *Chromium in the Natural and Human Environments*; Nriagu, J. O., Nieboer, E., Eds.; John Wiley & Sons: New York, 1988; Vol. 20, pp 21–79.
(14) Stollenwerk, K. G.; Grove, D. B. *J. Environ. Qual.* **1985**, *14*, 396–399.
(15) Rai, D.; Zachara, J. M. *Geochemical behavior of chromium species*; EPRI EA4544; Electric Power Research Institute: Palo Alto, CA, 1986.
(16) Fendorf, S. E.; Zasoski, R. J. *Environ. Sci. Technol.* **1992**, *26*, 79–85.
(17) Fendorf, S. E.; Fendorf, M.; Sparks, D. L.; Gronsky, R. *J. Colloid Interface Sci.* **1992**, *153*, 37–54.

(18) Fendorf, S. E.; Zasoski, R. J.; Burau, R. G. *Soil Sci. Soc. Am. J.* **1993**, *57*, 1508–1515.
(19) Bartlett, R.; James, B. R. *J. Environ. Qual.* **1979**, *8*, 31–35.
(20) Bartlett, R. J.; James, B. R. In *Chromium in the Natural and Human Environments*; Nriagu, J. O., Nieboer, E., Eds.; John Wiley & Sons: New York, 1988; Vol. 20, pp 267–304.
(21) Stumm, W.; Morgan, J. J. *Aquatic Chemistry*; John Wiley and Sons: New York, 1981; p 780.
(22) Sass, B. M.; Rai, D. *Inorg. Chem.* **1987**, *26*, 2228–2232.
(23) Bohn, H. L. *Soil Sci.* **1992**, *154* (5), 357–365.
(24) Weast, R. C., Ed. *CRC Handbook of Chemistry and Physics*; CRC Press, Inc.: Boca Raton, FL, 1988–1989.
(25) Eary, L. E.; Rai, D. *Environ. Sci. Technol.* **1988**, *22*, 972–977.
(26) Eary, L. E.; Rai, D. *Am. J. Sci.* **1989**, *289*, 180–213.
(27) Anderson, L. D.; Kent, D. B.; Davis, J. A. *Environ. Sci. Technol.* **1994**, *28*, 178–185.
(28) Sculley, J. C. *The Fundamentals of Corrosion*; Pergamon Press: New York, 1975; p 234.
(29) Evans, U. R. *The Corrosion and Oxidation of Metals: Scientific Principles and Practical Applications*; Edward Arnold (Publishers) Ltd.: London, 1960; p 1094.
(30) Snoeyink, V. L.; Jenkins, D. *Water Chemistry*; John Wiley and Sons: New York, 1980; p 463.
(31) Blowes, D. W.; Ptacek, C. J. *Subsurface Restoration Conference, Third International Conference on Ground Water Research*; National Center for Ground Water Research: Dallas, TX, 1992; pp 214–216.
(32) Powell, R. M.; Puls, R. W. Presented at Metal Speciation and Contamination of Aquatic Sediments Workshop, Jekyll Island, GA, 1993.
(33) Powell, R. M.; Puls, R. W.; Paul, C. J. *Innovative Solutions for Contaminated Site Management*; Water Environment Federation: Miami, FL, 1994; pp 485–496.
(34) Powell, R. M. M.S. Thesis, The University of Oklahoma, Norman, OK, 1994.
(35) Puls, R. W.; Paul, C. J.; Clark, D. A.; Vardy, J. *J. Soil Contam.* **1994**, *3*, 203–224.
(36) Adamson, A. W. *Physical Chemistry of Surfaces*; John Wiley and Sons: New York, 1990; p 777.
(37) Puls, R. W.; Powell, R. M.; Clark, D. A.; Paul, C. J. *Facilitated transport of inorganic contaminants in ground water: Part II. Colloidal transport*; EPA/600/M-91/040; U.S. Environmental Protection Agency, Robert S. Kerr Environmental Research Laboratory: Ada, OK, 1991.
(38) LeBlanc, D. R. In *Movement and Fate of Solutes in a Plume of Sewage-Contaminated Ground Water, Cape Cod, Massachusetts: U.S. Geological Survey Toxic Waste Ground-Water Contamination Program*; LeBlanc, D. R., Ed.; U.S. Geological Survey, Open-File Report 84-475; U.S. Geological Survey: Tucson, AZ, 1984; pp 1–9.
(39) Kleber, R. J.; Helz, G. R. *Environ. Sci. Technol.* **1992**, *26*, 307–312.
(40) Petrie, L.; Marozas, D.; Paulson, S.; Boucher, M. *Report to EPA R. S. Kerr Environmental Research Laboratory on Characterization of Elizabeth City Site Samples*; U.S. Department of the Interior, Bureau of Mines: Twin Cities Research Center Minneapolis, MN, 1993.
(41) Bohn, H. L.; McNeal, B. L.; O'Connor, G. A. *Soil Chemistry*; John Wiley & Sons: New York, 1979; p 329.
(42) Yong, R. N.; Mohamed, A. M. O.; Warkentin, B. P. *Principles of Contaminant Transport in Soils*; Elsevier Science Publishers B. V.: Amsterdam, The Netherlands, 1992; p 327.
(43) James, B. R.; Bartlett, R. J. *J. Environ. Qual.* **1983**, *12*, 177–181.
(44) Stollenwerk, K. G.; Grove, D. B. *J. Environ. Qual.* **1985**, *14*, 150–155.
(45) Asikainen, J. M.; Nikolaidis, N. P. *Ground Water Monit. Remed.* **1994**, 185–191.
(46) Puls, R. W.; Powell, R. M.; Clark, D.; Eldred, C. J. *Water, Air, Soil Pollut.* **1991**, *57–58*, 423–430.
(47) Zachara, J. M.; Girvin, D. C.; Schmidt, R. L.; Resch, C. T. *Environ. Sci. Technol.* **1987**, *21*, 589–594.
(48) Pourbaix, M. *Atlas of Electrochemical Equilibria in Aqueous Solutions*; Pergamon Press: Oxford, 1966.
(49) Chou, L.; Wollast, R. *Geochim. Cosmochim. Acta* **1984**, *48*, 2205–2207.
(50) Chou, L.; Wollast, R. *Am. J. Sci.* **1985**, *285*, 963–993.
(51) Powell, R. M.; Puls, R. W.; Hightower, S. K.; Clark, D. A. Presented at American Chemical Society 209th Annual National Meeting, Special Symposium on Contaminant Remediation with Zero-Valent Metals, Anaheim, CA, 1995; *Natl. Meet.—Am. Chem. Soc., Div. Environ. Chem.* **1995**, *35*, 784–787.
(52) Velleman, P. F. *DataDesk®, The New Power of Statistical Vision Handbook*; Data Description, Inc.: Ithaca, NY, 1992.
(53) Glasstone, S. *Textbook of Physical Chemistry*; D. Van Nostrand Company: New York, 1946; p 1320.
(54) Levy, R. A. *Principles of Solid State Physics*; Academic Press: New York, 1968; p 464.

Received for review September 6, 1994. Revised manuscript received February 15, 1995. Accepted April 25, 1995.[⊗]

ES940557C

[⊗] Abstract published in *Advance ACS Abstracts,* June 1, 1995.